Growth and characterization of $ZnO_{1-x}S_x$ highly mismatched alloys over the entire composition

M. Jaquez,[1,2] K. M. Yu,[1,3] M. Ting,[1,2] M. Hettick,[4,5] J. F. Sánchez-Royo,[6] M. Wełna,[1,7] A. Javey,[4,5] O. D. Dubon,[1,8] and W. Walukiewicz[1,a)]
[1]*Materials Sciences Division, Lawrence Berkeley National Laboratory, Berkeley, California 94720, USA*
[2]*Department of Mechanical Engineering, University of California, Berkeley, California 94720, USA*
[3]*Department of Physics and Materials Science, City University of Hong Kong, Kowloon, Hong Kong*
[4]*Department of Electrical Engineering and Computer Sciences, University of California, Berkeley, California 94720, USA*
[5]*Joint Center for Artificial Photosynthesis, Lawrence Berkeley National Laboratory, Berkeley, California 94720, USA*
[6]*ICMUV, Instituto de Ciencia de Materiales, Universitat de València, P.O. Box 22085, 46071 Valencia, Spain*
[7]*Department of Experimental Physics, Wrocław University of Technology, Wybrzeze Wyspianskiego 27, 50-370 Wrocław, Poland*
[8]*Department of Materials Science and Engineering, University of California, Berkeley, California 94720, USA*

(Received 25 August 2015; accepted 13 November 2015; published online 1 December 2015)

Alloys from ZnO and ZnS have been synthesized by radio-frequency magnetron sputtering over the entire alloying range. The $ZnO_{1-x}S_x$ films are crystalline for all compositions. The optical absorption edge of these alloys decreases rapidly with small amount of added sulfur ($x \sim 0.02$) and continues to red shift to a minimum of 2.6 eV at $x = 0.45$. At higher sulfur concentrations ($x > 0.45$), the absorption edge shows a continuous blue shift. The strong reduction in the band gap for O-rich alloys is the result of the upward shift of the valence-band edge with x as observed by x-ray photoelectron spectroscopy. As a result, the room temperature bandgap of $ZnO_{1-x}S_x$ alloys can be tuned from 3.7 eV to 2.6 eV. The observed large bowing in the composition dependence of the energy bandgap arises from the anticrossing interactions between (1) the valence-band of ZnO and the localized sulfur level at 0.30 eV above the ZnO valence-band maximum for O-rich alloys and (2) the conduction-band of ZnS and the localized oxygen level at 0.20 eV below the ZnS conduction band minimum for the S-rich alloys. The ability to tune the bandgap and knowledge of the location of the valence and conduction-band can be advantageous in applications, such as heterojunction solar cells, where band alignment is crucial. © *2015 AIP Publishing LLC*.
[http://dx.doi.org/10.1063/1.4936551]

I. INTRODUCTION

The high demand and need for renewable energy have triggered a vast exploration of potential materials for energy applications. Zinc oxide (ZnO) is a material of great interest because it is non-toxic, earth abundant, and relatively inexpensive.[1] ZnO has great potential for high power electronics, ultra violet optical devices, and transparent conductors for photovoltaic applications due to its wide bandgap of 3.3 eV.[2] Zinc sulfide (ZnS) is another wide bandgap semiconductor with a bandgap of 3.6–3.8 eV that is currently used in optoelectronic devices such as blue light-emitting diodes and n-window layers for thin-film solar cells.[3]

It has been found that alloying ZnO with ZnS allows the room-temperature bandgap of ZnO to be modified,[2,4–7] making it useful as a material for solar applications.[8–11] Despite various reports on the growth of $ZnO_{1-x}S_x$ alloys, only limited information is known about their electronic structures.[10] A better understanding of the band structure and offsets with other semiconductors is essential for device applications using these $ZnO_{1-x}S_x$ alloys. One potential application for these $ZnO_{1-x}S_x$ alloys is replacing the toxic cadium sulfide (CdS) buffer layer in copper indium gallium selenide (CIGS) and copper zinc tin sulfide (CZTS) solar cells. Various reports have replaced the CdS layer with $ZnO_{1-x}S_x$ alloys, but not knowing the position of the conduction band has made it difficult to choose a composition for the best conduction band alignment.[11]

$ZnO_{1-x}S_x$ alloys can be classified as highly mismatched alloys (HMAs), semiconductor compounds where the anions are partially substituted with isovalent atoms of considerably different size and/or electronegativity. The electronic band structure of HMAs is well described by the band anticrossing (BAC) model that considers an interaction between localized states introduced by the minority anions and the extended states of the host conduction/valence band in the dilute alloy composition limit. Well-known HMAs that have been shown to follow the framework of the BAC model include GaN_xAs_{1-x}, ZnO_xTe_{1-x}, and $ZnO_{1-x}Se_x$.[12,13] In this paper, we synthesized $ZnO_{1-x}S_x$ alloys over the entire composition range and investigated their optical properties as well as the electronic band structures. The changes in optical properties of $ZnO_{1-x}S_x$ are explained by the anticrossing interactions between localized foreign atoms and the extended conduction/valence band states of the ZnO/ZnS hosts.

a)Author to whom correspondence should be addressed. Electronic mail: w_walukiewicz@lbl.gov

II. EXPERIMENTAL METHODS

$ZnO_{1-x}S_x$ alloy thin films were deposited on glass and sapphire substrates at 240 °C using radio-frequency magnetron sputtering. Adjusting the sputtering power and target-substrate distance for two separate ZnO and ZnS targets controlled the alloy compositions of the films. The film thickness and composition were measured by Rutherford backscattering spectrometry (RBS) using a 3 MeV He^{2+} ion beam. Film structure and crystallinity were studied by X-ray diffraction (XRD). The concentration of substitutional sulfur in ZnO (or oxygen in ZnS) was calculated from shifts in the XRD (0002) peak using a linear extrapolation of the lattice parameter between that of wurtzite ZnO ($c = 0.52$ nm) and ZnS ($c = 0.626$ nm) (Vegard's Law).[14] Note that this may be different from RBS results since RBS measures the total elemental composition in the films. Absorption coefficients (α) of the alloy films were obtained by transmission and reflection spectra measured over the photon energy range of 0.5–5.0 eV. The bandgaps of the dilute sulfur (oxygen) samples were determined by fitting the absorption coefficient spectra using the valence BAC (VBAC)[13] and the conduction BAC (CBAC)[15] model, respectively. Bandgaps of alloys with compositions in the range of $0.16 < x < 0.9$ were estimated by the extrapolation of the square of absorption coefficient, α, assuming parabolic dispersion relations. O-rich samples with $x < 0.27$ were examined by X-ray photoelectron spectroscopy (XPS) in order to verify shifts in the valence-band maximum and to estimate the sulfur composition with the relative intensities between the Zn2p and S2p peaks. XPS spectra were measured using a monochromated Al K_α X-ray source ($h\nu = 1486.6$ eV) with a hemispherical electron analyzer. XPS spectra were charge corrected to the adventitious C1s spectral component binding energy.[16]

III. RESULTS AND DISCUSSION

All films grown on glass were textured along the c axis and only the (0002) diffraction peak is visible in the XRD patterns. Figure 1 shows XRD (0002) diffraction peaks for select $ZnO_{1-x}S_x$ films across the composition range. We note that ZnS exists in both zinc-blende and wurtzite structures. The structure of the S-rich films was not determined since the $(111)_{zincblende}$ peak coincides with the $(0002)_{wurtzite}$ peak of ZnS. Using grazing incidence phi scans Meyer *et al.*[4] reported a wurtzite structure for $ZnO_{1-x}S_x$ films throughout the composition range. Because our $ZnO_{1-x}S_x$ films were synthesized using a similar method, they likely crystallize in the wurtzite structure as well. The XRD results show a monotonic shift of the $(0002)_{wurtzite}$ ZnO reflection towards smaller 2θ with increasing sulfur content. This indicates an increase of the lattice parameter of $ZnO_{1-x}S_x$ as expected due to the substitution of larger S atoms with O. Using Vegard's law, the composition of the alloy can be determined.

The concentration of sulfur determined through RBS and XRD using Vegard's law are compared in Fig. 2. The good agreement of alloy composition measured by XRD and RBS suggests that all the samples are, indeed, random alloys with S and O in the group VI sublattice. XPS was also used

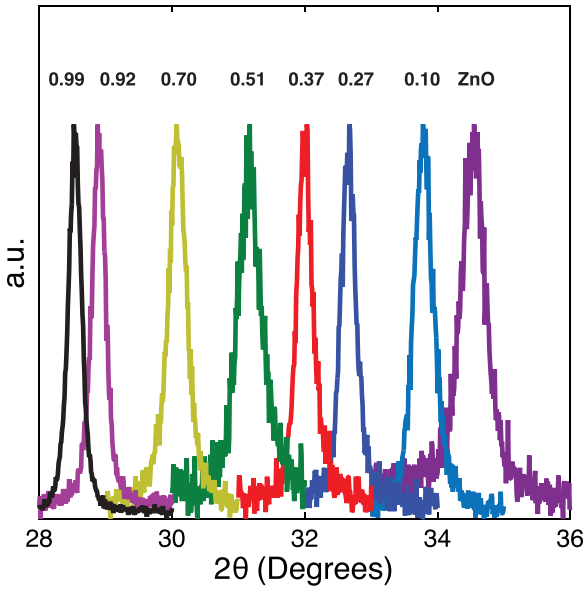

FIG. 1. Normalized XRD (0002) diffraction peak of $ZnO_{1-x}S_x$ alloys over nearly the entire composition range (x from 0 to 0.99). The composition listed on the diffraction peaks was found using Vegard's law.

to estimate the surface concentration of sulfur. The XPS spectra for several samples in the binding energy range of the Zn and S 2p peaks are shown in Figs. 3(a) and 3(b), respectively. The intensity of $Zn2p_{3/2}$ and $S2p_{3/2}$ photoemission peaks was normalized with atomic cross sections. The surface sulfur content in the films (1–10 nm) was estimated from the relative intensity of the S2p peaks. The concentration of sulfur calculated from RBS, XRD, and XPS for a few samples are shown in Table I. The surface composition found through XPS differs by only a few percent from the composition found using RBS and XRD. This implies that the composition of a film is uniform throughout its thickness. Strain might be a reason why XRD values may be a few percent higher than RBS results. Previous results for $ZnO_{1-x}Se_x$ showed that tensile strain in the films accounted for a +3%

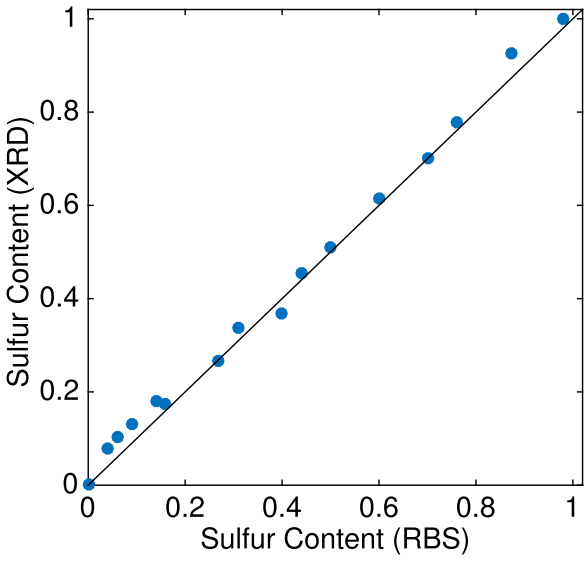

FIG. 2. Comparison between RBS and XRD calculated concentration of sulfur.

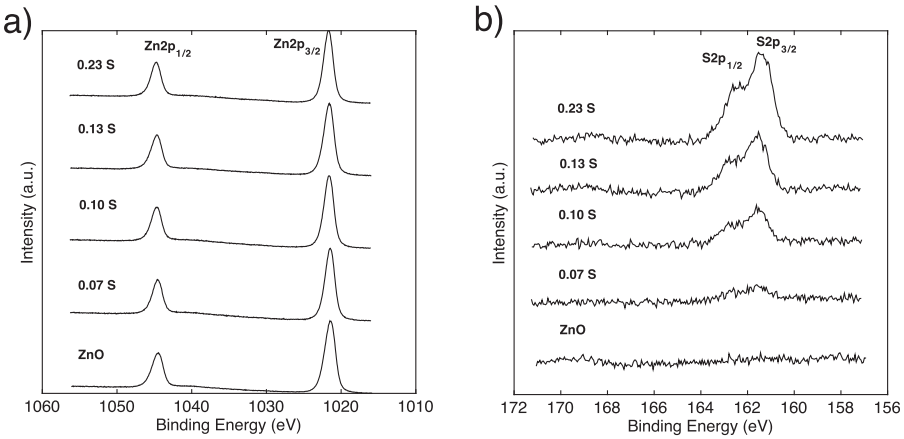

FIG. 3. (a) XPS Zn2p spectra of several films, (b) XPS S2p spectra of several films. The composition listed is the surface composition found using the Zn2p and S2p XPS spectra.

difference in the Se composition determined using XRD compared to RBS.[17] Using RBS, the elemental composition of samples has an estimated accuracy of ~1%.[18] Using XPS, an accuracy of 10% is typically quoted.[19]

In order to characterize the effects of sulfur incorporation on the electronic structure of the $ZnO_{x-1}S_x$ alloys, valence-band spectra by XPS were collected for a range of compositions from pure ZnO to 0.27 sulfur as measured by RBS (see Fig. 4). The pure ZnO material has the top of the valence band composed of O2p states. The introduction of sulfur in the alloys causes a shift of the valence band closer to the Fermi level with increasing S concentration as well as a depression in the slope of the band edge. The surface sensitivity of XPS allows to relate the observed shifts to a common energy reference since the Fermi level at the surface of each sample is located at the Fermi Level stabilization energy (E_{FS}), ~4.9 eV below vacuum level in all semiconductors.[20] Comparing the spectra measured for ZnO and the alloy films in Fig. 3(b), one sees that S incorporation into the ZnO lattice increases the intensity of the S 2p peaks without any appreciable energy shift. The Zn2p peaks in Fig. 3(a) do not broaden or shift in energy for the samples measured, indicating that the upward shifting of the valence band is due to the incorporation of S and not defects.[21] Therefore, as the sulfur concentration increases, the density of states increases above the valence band (VB) of ZnO.[22] Since the conduction band (CB) minimum of ZnO is located close to E_{FS}, the binding energy measured through XPS is close to the bandgap of ZnO.

The absorption spectra for samples with S <0.27 or O <0.11 films are shown in Fig. 5. The incorporation of sulfur into the ZnO matrix results in a shift of the absorption edge from ultraviolet into the visible spectrum (Fig. 5(a)). Substituting S into the O sublattice in ZnO introduces a localized level close to the valence band edge of ZnO. The interaction of the localized S level with the extended valence-band states of ZnO results in VBAC effect when a significant amount of S atoms are incorporated into the lattice. When this occurs, the valence band splits into two subbands (E_+ and E_-). On the other hand, incorporation of O into ZnS matrix leads to a red shift in the absorption edge (Fig. 5(b)). In this case, oxygen forms a localized level at ~0.2 eV below the conduction band of ZnS,[23] resulting in CBAC, splitting the conduction band into two subbands (E_+ and E_-). These anticrossing effects at the dilute S (dilute O) compositions produce narrow, non-parabolic S (O) derived bands with the total number of states dependent on the S (O) content. Hence, estimating the bandgap of these alloys using the conventional method of extrapolating α^2 to zero will result in significant error. Here, we adopt the procedure based on the BAC model previously used to fit absorption curves in $ZnO_{1-x}Se_x$ and $ZnO_{1-x}Te_x$ HMAs.[13,24] The dispersion relations for the E_+ and E_- subbands are given by

TABLE I. Concentration of Sulfur found by RBS, XRD, and XPS.

Sample Name	RBS	XRD	XPS
ZnO	0	0	0
R497	0.04	0.07	0.08
R498	0.09	0.10	0.01
R487	0.16	0.17	0.13
R488	0.27	0.27	0.23

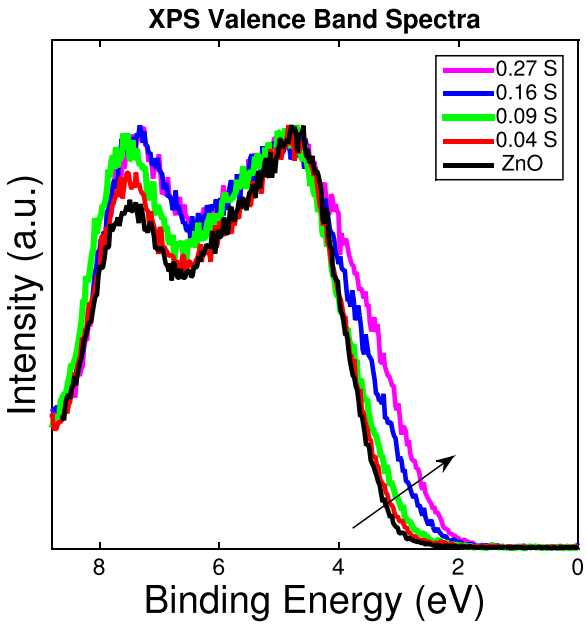

FIG. 4. XPS valence band spectra for x < 0.27, the compositions listed were found through RBS. The arrow indicates the monoatomic upward shift in the valence band as sulfur content increases.

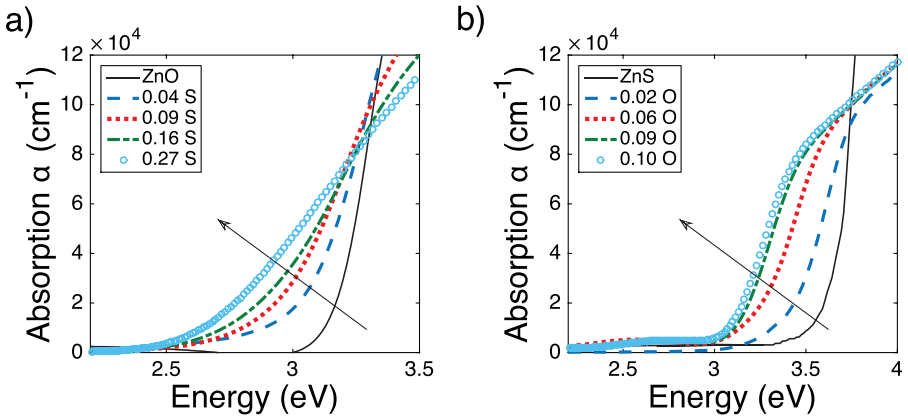

FIG. 5. (a) Absorption spectra for select films with dilute sulfur in a ZnO matrix, the arrow indicates the direction the absorption edge shifts with the increase in sulfur content. (b) Absorption spectra for select films with dilute oxygen in a ZnS matrix, the arrow indicates the direction the absorption edge shifts with an increase in oxygen content. The compositions listed were found through RBS.

$$E_{\pm} = \frac{1}{2}\left[(E_d + E(k)) \pm \sqrt{(E(k) - E_d)^2 + 4C^2x}\right], \quad (1)$$

where E_d refers to the level of the localized states of the minority anion, $E(k)$ corresponds to the dispersion relation of the band that is undergoing an anticrossing effect (i.e., valence band of ZnO or the conduction band of ZnS), C is the coupling parameter which represents the coupling strength between the localized and delocalized states, and x is the concentration of the minority substitutional anions.

A. Valence band anticrossing: Absorption fitting

As mentioned previously, the VBAC effect occurs when sulfur substitutes oxygen in the ZnO rich side. We adopt the simplified version of the VBAC[13] that represents the BAC model given by Equation (1). In this case, $E_d = E_S$ is the energy of the localized S level above the ZnO valence band edge, $E(k) = E_V(k)$ is the ZnO matrix valence band dispersion, $C = C_{VB}$ is the coupling parameter, and x is the S composition. We take into consideration optical transitions from 3-fold degenerate valence bands including the spin orbit split off band to the conduction band with the spin orbit splitting energy of S.[25] Therefore, to calculate the absorption coefficient, we consider three optical transitions: the S derived band to conduction band $[E_+(k)]$, the S spin orbit split band to conduction band $[E_+^{SO}(k)]$, and the heavy and light hole derived bands of the ZnO matrix to conduction band $[E_-(k)]$.

The optical joint-density of states (JDOS) were convolved with a Gaussian function at each wave vector, k, an approach used in Ref. 17 to account for the broadening in the bands. Therefore, the optical absorption coefficient from a single valence band, e.g., $[E_+(k)]$, can be written as an integral of the JDOS with respect to k

$$g_+(\hbar\omega) = \int_{-\frac{\pi}{a}}^{\frac{\pi}{a}} \left[-\sin\left(\frac{\theta(k)}{2}\right)\right]^2 \frac{1}{\Delta_+\sqrt{2\pi}} \times \exp\left(-\frac{\left(\hbar\omega - \left[E_C(k) - E_+(k)\right]\right)^2}{2\Delta_+^2}\right) k^2 dk, \quad (2)$$

where $g_+(\hbar\omega)$ is in terms of the number of states per unit volume per unit frequency, $E_C(k)$ is the conduction band dispersion, the first term under the integral represents the fraction of the contribution of the delocalized states to the optical transition, where

$$\theta(k) = \tan^{-1}\left(\frac{2C\sqrt{x}}{E_d - E_V(k)}\right), \quad (3)$$

and Δ_+ is the broadening parameter. The limits of integration are from $\frac{\pi}{a}$ to $-\frac{\pi}{a}$ (in units of cm^{-1}), which represents the first Brillion zone, where a is the lattice constant. The expression for the calculated total absorption coefficient includes the three transitions discussed above, with each transition weighted by their degeneracy factor

$$\alpha(\hbar\omega) = \alpha_0\left[\frac{2}{3}g_+(\hbar\omega) + \frac{1}{3}g_{+,so}(\hbar\omega) + g_-(\hbar\omega)\right], \quad (4)$$

where α_0 is an overall scaling constant. The coupling parameter, C_{VB}, scaling constant, α_0, and the localized S level, E_S were found by fitting the absorption curve of the sample with the lowest sulfur content. This approach was used, since the highest anti-crossing interaction is expected at low sulfur content. These three values were kept constant for the remaining samples to find the broadening parameters for each transition (Δ_+, Δ_-, Δ_{+SO}). The best-fit broadening parameters were found by minimizing the root mean square error between the experimental absorption curve and the calculated absorption.

Figure 6(a) shows the experimental result and the fitting of the absorption coefficient using the VBAC for the 0.04 sulfur film, which also shows the three optical transition contributions. These fittings were done for all the dilute sulfur samples and it was possible to extract the sulfur level, E_S, of 0.30 eV above the valence band edge of ZnO and the coupling parameter, C_{VB} of 0.60 eV. These values are consistent with previous reports on $ZnO_{1-x}Se_x$ where the selenium level was found to be 0.90 eV above the ZnO valence band edge, and the coupling parameter was found to be 1.2 eV.[13,26] Since the difference in electronegativity and ion size is smaller between sulfur and oxygen than the difference between selenium and oxygen, a smaller coupling parameter is expected. Using the coupling parameter, and the sulfur level, it was possible to calculate the band structure (Fig. 6(b)) and determine the bandgap of the $ZnO_{1-x}S_x$ alloys from the maximum of the E_+ subband to the conduction band minimum. The observed upward shift of the VB edge is in a good qualitative

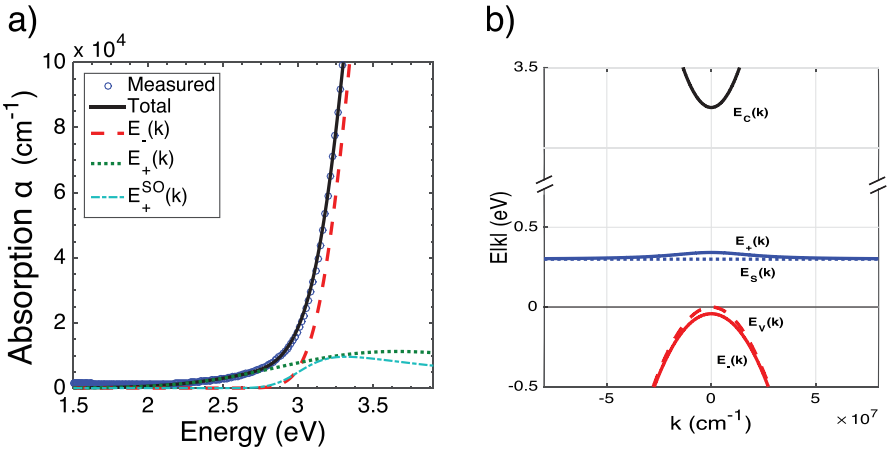

FIG. 6. (a) Measured absorption spectra for 0.04 sulfur film (determined by RBS) and the calculated theoretical fit using the VBAC model. The separate absorption contributions are also shown. The sulfur level is 0.30 eV above the ZnO valence band and the coupling parameter, C_{VB}, is 0.60 eV. (b) Calculated band structure for the 0.04 sulfur film.

agreement with the XPS data of Fig. 4 that clearly show an appearance of additional density of states above the VB edge of ZnO. This method for calculating the bandgap was used for samples with sulfur content less than 0.14.

B. Conduction band anticrossing: Absorption fitting

The CBAC effect was used to obtain the composition dependence of the bandgap for $ZnO_{1-x}S_x$ samples with dilute amount of O substituting S. In this case, E_d in Equation (1) is the energy of the localized O level E_O, $E(k) = E_c(k)$ is the ZnS matrix conduction band dispersion, $C = C_{CB}$ is the coupling parameter, and x is the O composition. Here, we consider only two optical transitions: the valence band to the O derived band $[E_-(k)]$, and the valence band to the ZnS matrix derived band $[E_+(k)]$. Therefore, the expression for the calculated total absorption coefficient includes the two transitions discussed above, with each transition weighted by their degeneracy factor

$$\alpha(\hbar\omega) = \alpha_0[g_+(\hbar\omega) + g_-(\hbar\omega)], \tag{5}$$

where α_0 is an overall scaling constant. By fitting the experimental absorption coefficient using Equation (1), a coupling parameter C_{CB} of 1.50 eV was obtained. Note that the coupling parameter reported here is 10% larger than the value of $C_{CB} = 1.35$ eV reported previously for dilute oxygen $ZnO_{1-x}S_x$ alloys.[27] The location of the localized O level was fixed to $E_O = 3.5$ eV above the ZnS valence band as previously found in Ref. 23. Figure 7(a) shows the experimental result and the fitting of the absorption coefficient using CBAC for the 0.02 oxygen film (0.98 sulfur), which also shows the two optical transition contributions. Figure 7(b) shows the calculated band structure that was used to determine the bandgap of the $ZnO_{1-x}S_x$ alloys from the valence band maximum to the E_- subband minimum. This method for calculating the bandgap was used for samples with oxygen content less than 0.10 (sulfur content more than 0.90).

C. Bandgap dependence on composition

Using the values of E_S, C_{VB}, and C_{CB} obtained in this work and the known E_O value, we also calculated the dependence of the conduction band and valence band edges of the $ZnO_{1-x}S_x$ alloys across the whole composition range. These calculations were performed using the compositional weighting method proposed in Ref. 28 and the results are shown in Fig. 8. The BAC calculations show that the reduction in the band gap of O- and S-rich $ZnO_{1-x}S_x$ films is due to the upward movement of the valence band and the downward movement of the conduction band, respectively.

In Fig. 8(b), the bandgaps calculated from: (1) the absorption fitting using valence BAC for samples with sulfur $x < 0.16$ (green filled circles), (2) linear extrapolation of the square of absorption coefficient (α^2) for samples with $0.16 > x < 0.90$ sulfur (blue open circles), and (3) the

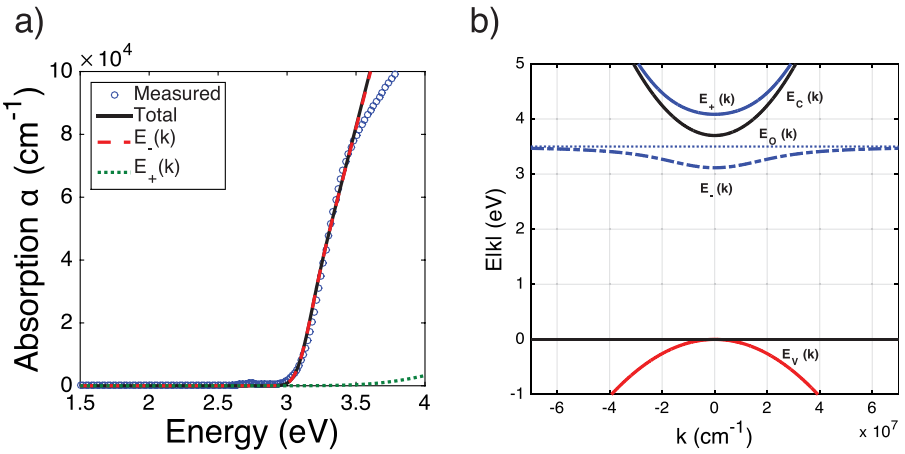

FIG. 7. (a) Measured absorption spectra for 0.10 oxygen film (determined by RBS) and the calculated total absorption using the CBAC model. The separate absorption contributions are also shown. The coupling parameter, C_{CB}, is 1.5 eV. (b) Calculated band structure for the 0.10 oxygen film.

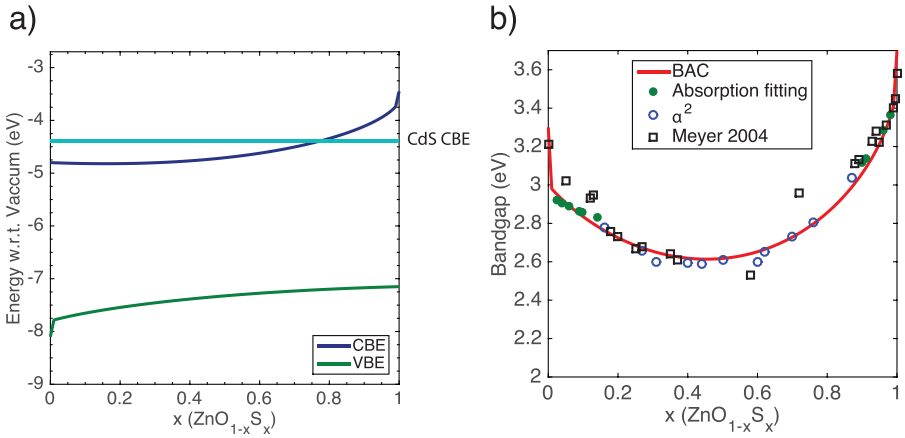

FIG. 8. (a) Calculated conduction band and valence band edges. (b) Composition dependence of the bandgap of $ZnO_{1-x}S_x$ alloys. BAC line was determined by subtracting the calculated valence band edge from the calculated conduction band edge shown in (a). The experimental bandgaps found using the absorption fittings are plotted alongside the experimental data of Meyer *et al.*[4]

absorption fitting using conduction BAC for samples with $x > 0.90$ sulfur (green filled circles). The compositional weighting method is labeled as BAC since it utilizes the values E_S, C_{VB}, C_{CB}, determined through the absorption fittings described earlier. The bandgaps found in this work are plotted alongside the experimental data found in Ref. 4 labeled as open black squares. It can be noted that in the dilute S region, the bandgaps reported in Ref. 4 deviate from the calculated BAC bandgap and the absorption fitting bandgaps. This indicates that using the standard method to determine the band gap from the extrapolation of α^2 leads to significant error due to the non-parabolic dispersion of the S-derived at dilute S contents. In the middle region, it is assumed that at higher sulfur content the S-derived band becomes more delocalized thus becoming more parabolic, making the standard method (α^2) valid in this region. There is good agreement between the BAC, α^2, and the values reported in Ref. 4.

D. CdS layer replacement in thin-film solar cells

These $ZnO_{1-x}S_x$ alloys are of interest as they offer a possibility to tune not only the band gap but also more importantly the valence band and conduction band edges, specifically through alloying. In Fig. 8(a), the conduction-band edge of CdS is illustrated showing that it lies between the conduction-band edge of ZnO and ZnS. Therefore, with alloying, it is possible to align the conduction band edge of a $ZnO_{1-x}S_x$ alloy to that of CdS. From the calculated valence-band and conduction-band edges in Fig. 8(a), we have determined that the composition of $ZnO_{1-x}S_x$ for which its conduction-band edge aligns to that of CdS is $x \sim 0.75$. $ZnO_{0.25}S_{0.75}$ has a bandgap of ~2.8 eV, the larger bandgap of this alloy compared to CdS (2.4 eV) will allow more light to penetrate the absorber layer that can lead to an increase in efficiency as more light energy can be converted into electricity. Replacing CdS in thin film solar cells is of interest due to the toxicity of cadmium, since cadmium is one of the most toxic metals. Cadmium containing solar cells currently have stringent recycling procedures for this matter.[29]

IV. CONCLUSIONS

ZnO_xS_{1-x} films were synthesized over the whole composition range using radio frequency magnetron sputtering. ZnO and ZnS are miscible and alloys from them are likely isocrystalline (wurtzite) for all compositions. The bandgap of $ZnO_{1-x}S_x$ was tuned from 3.7 eV down to 2.6 eV, and the band anticrossing model explains these optical results. Fitting the absorption coefficient of this system, the coupling parameters and the S localized level within the ZnO band gap were found. These values were used to predict the energies of the conduction band and the valence band edges relative to the vacuum level. The conduction band of a 0.75 S film was found to align with the conduction band of CdS potentially enabling the ability to replace the toxic layer in thin film solar cells. Tuning of the conduction band for these alloys is advantageous for solar applications.

ACKNOWLEDGMENTS

This work was supported by the Director, Office of Science, Office of Basic Energy Sciences, Materials Sciences and Engineering Division, of the U.S. Department of Energy under Contract No. DE-AC02-05CH11231. M.J. acknowledges support from the NSF Bridge to the Doctorate Fellowship and thanks Professor Chris Dames for his feedback on this work. J.F.S.R. acknowledges financial support from the Mobility Program of VLC-CAMPUS. M.W. acknowledges the financial support from the National Science Centre through grant ETIUDA No. 2013/08/T/ST3/00400.

[1]M. D. McCluskey and S. J. Jokela, J. Appl. Phys. **106**, 071101 (2009).
[2]H. L. Pan, T. Yang, B. Yao, R. Deng, R. Y. Sui, L. L. Gao, and D. Z. Shen, Appl. Surf. Sci. **256**, 4621 (2010).
[3]P. Roy, J. R. Ota, and S. K. Srivastava, Thin Solid Films **515**, 1912 (2006).
[4]B. K. Meyer, A. Polity, B. Farangis, Y. He, D. Hasselkamp, T. Kramer, and C. Wang, Appl. Phys. Lett. **85**, 4929 (2004).
[5]C. Persson, C. Platzer-Björkman, J. Malmström, T. Törndahl, and M. Edoff, Phys. Rev. Lett. **97**, 146403 (2006).
[6]Y. Z. Yoo, Z. W. Jin, T. Chikyow, T. Fukumura, M. Kawasaki, and H. Koinuma, Appl. Phys. Lett. **81**, 3798 (2002).
[7]X. F. Fan, Z. X. Shen, Y. M. Lu, and J. L. Kuo, New J. Phys. **11**, 093008 (2009).
[8]T. Minemoto, A. Okamoto, and H. Takakura, Thin Solid Films **519**, 7568 (2011).
[9]A. Okamoto, T. Minemoto, and H. Takakura, Jpn. J. Appl. Phys., Part 1 **50**, 04DP10 (2011).
[10]S. Sharbati and J. R. Sites, IEEE J. Photovoltaics **4**, 697 (2014).
[11]K. Ramanathan, J. Mann, S. Glynn, S. Christensen, J. Pankow, J. Li, J. Scharf, L. Mansfield, M. Contreras, and R. Noufi, *2012 IEEE 38th Photovoltaic Specialists Conference (PVSC)* (2012), p. 001677.
[12]K. Alberi, J. Wu, W. Walukiewicz, K. M. Yu, O. D. Dubon, S. P. Watkins, C. X. Wang, X. Liu, Y. J. Cho, and J. Furdyna, Phys. Rev. B **75**, 045203 (2007).

[13]M. A. Mayer, D. T. Speaks, K. M. Yu, S. S. Mao, E. E. Haller, and W. Walukiewicz, Appl. Phys. Lett. **97**, 022104 (2010).
[14]M. Grünwald, A. Zayak, J. B. Neaton, P. L. Geissler, and E. Rabani, J. Chem. Phys. **136**, 234111 (2012).
[15]R. Broesler, E. E. Haller, W. Walukiewicz, T. Muranaka, T. Matsumoto, and Y. Nabetani, Appl. Phys. Lett. **95**, 151907 (2009).
[16]P. Swift, Surf. Interface Anal. **4**, 47 (1982).
[17]M. A. Mayer, Ph.D. Dissertation, Department of Materials Science and Engineering, University of California, Berkeley, 2012.
[18]C. Jeynes, Z. H. Jafri, R. P. Webb, A. C. Kimber, and M. J. Ashwin, Surf. Interface Anal. **25**, 254 (1997).
[19]R. Hesse, P. Streubel, and R. Szargan, Surf. Interface Anal. **37**, 589 (2005).
[20]D. M. Detert, K. B. Tom, C. Battaglia, J. D. Denlinger, S. H. N. Lim, A. Javey, A. Anders, O. D. Dubon, K. M. Yu, and W. Walukiewicz, J. Appl. Phys. **115**, 233708 (2014).
[21]Y. F. Li, B. Yao, Y. M. Lu, B. H. Li, Y. Q. Gai, C. X. Cong, Z. Z. Zhang, D. X. Zhao, J. Y. Zhang, D. Z. Shen, and X. W. Fan, Appl. Phys. Lett. **92**, 192116 (2008).
[22]P. D. C. King, T. D. Veal, A. Schleife, J. Zúñiga-Pérez, B. Martel, P. H. Jefferson, F. Fuchs, V. Muños-Sanjosé, F. Bechstedt, and C. F. McConville, Phys. Rev. B **79**, 205205 (2009).
[23]K. Yu, W. Walukiewicz, J. Wu, W. Shan, J. W. Beeman, M. A. Scarpulla, O. D. Dubon, and P. Becla, Phys. Rev. Lett. **91**, 246403 (2003).
[24]M. Ting, R. dos Reis, M. Jaquez, O. D. Dubon, S. S. Mao, K. M. Yu, and W. Walukiewicz, Appl. Phys. Lett. **106**, 092101 (2015).
[25]J. E. Peralta, J. Heyd, G. E. Scuseria, and R. L. Martin, Phys. Rev. B **74**, 073101 (2006).
[26]M. A. Mayer, K. M. Yu, D. T. Speaks, J. D. Denlinger, L. A. Reichertz, J. W. Beeman, E. E. Haller, and W. Walukiewicz, J. Phys. Chem. C **116**, 15281 (2012).
[27]M. Wełna, R. Kudrawiec, Y. Nabetani, T. Tanaka, M. Jaquez, O. D. Dubon, K. M. Yu, and W. Walukiewicz, Semicond. Sci. Technol. **30**, 085018 (2015).
[28]J. Wu, W. Walukiewicz, K. M. Yu, J. Ager, E. E. Haller, I. Miotkowski, A. Ramdas, C. H. Su, I. Sou, R. Perera, and J. Denlinger, Phys. Rev. B **67**, 035207 (2003).
[29]K. W. Böer, Energy Convers. Manage. **52**, 426 (2011).